Letter

Uncovering hidden chiral symmetry in nonbipartite kagome and pyrochlore lattices with spin-orbit coupling by the Wilson loop

Hiroki Nakai [ORCID],[1,*] Masataka Kawano,[1,2] and Chisa Hotta [ORCID][1,†]

[1]*Graduate School of Arts and Sciences, University of Tokyo, Meguro-ku, Tokyo 153-8902, Japan*
[2]*Department of Physics, Technical University of Munich, 85748 Garching, Germany*

Chiral symmetry (CS) in energy bands appears as perfectly symmetric antibonding and bonding pairs of energy levels. It has only been observed in a few classes of models when bipartite hopping occurs among their pairwise bases. We find that *nonbipartite* kagome and pyrochlore lattices can host CS when strong spin-orbit coupling is introduced. Unfortunately, the model exhibits an intricate frustrated hopping accompanied by spin rotation with no apparent sign of realizing CS. However, by making use of a local gauge transformation that properly rotates the spin quantization axis site-dependently, complex hopping among up- and down-spin electrons is untangled to bipartite-hopping ones. The clue to find such a transformation and to construct a chiral operator is given by the gauge invariant Wilson loop operator on a triangular unit. The framework allows us to disclose the symmetry and structures of spin-textured CS wave functions and energy bands.

Introduction. Electronic phases of matter are very often discussed and tabulated in terms of symmetries. Space group symmetries combined with time-reversal symmetry (TRS) classify the electronic band structures and the possible choices of symmetry-broken phases [1,2]. Whereas, the periodic table developed for topological insulators (TIs) and superconductors has revealed that the symmetries that protect and distinguish them are not the spatial ones but are TRS, particle-hole symmetry (PHS), and chiral symmetry (CS) [3,4]. The three symmetries generate a total of ten symmetry classes, which are further extended to include spatial symmetries [5].

The CS is identified as a diphycercal energy spectrum and is present when TRS and PHS are both broken or both unbroken. It helps to elucidate the nature of topological phases [6]. For example, the winding number in the Su-Schrieffer-Heeger model [7–9] is defined using the CS operator, and the number of singular zero-mode Landau levels and the bulk-edge correspondence of graphene [10–12] are understood using CS. It explains the Dirac points or semimetals of bilayer graphene [13–15]. A more important physical consequence of CS is to support the zero-energy flat bands in twisted bilayer graphene or its analog [16–20], which is the possible source of correlated superconductivity [21,22].

Despite its importance, CS is observed only in restricted classes of models; the bipartite lattice model [23–25], the Bogoliubov–de Gennes (BdG) Hamiltonian with TRS and conserved magnetization, and the quantum chromodynamics models [26]. How this symmetry could emerge in wider classes of physical systems is an important question. Here, we discover that the noninteracting fermions on a *nonbipartite*

lattice with strong spin-orbit coupling (SOC) can host CS bands. We further prove that the gauge invariant Wilson loop operator [27] serves as a detector of CS, and using the Wilson loop operator, obtain an explicit form of the chiral operator.

Chiral symmetry. Without loss of generality, the low-energy effective Hamiltonian in momentum space is described by the quadratic Hamiltonian given as $\mathcal{H} = \sum_{\boldsymbol{k}} \boldsymbol{c}_{\boldsymbol{k}}^{\dagger} \mathcal{H}(\boldsymbol{k}) \boldsymbol{c}_{\boldsymbol{k}}$, where $\boldsymbol{c}_{\boldsymbol{k}}^{\dagger} = (c_{\boldsymbol{k}1\uparrow}^{\dagger}, c_{\boldsymbol{k}1\downarrow}^{\dagger}, \ldots, c_{\boldsymbol{k}n\uparrow}^{\dagger}, c_{\boldsymbol{k}n\downarrow}^{\dagger})$ are the set of creation operators of a Bloch electron with spin $(\uparrow, \downarrow)$ and wave vector $\boldsymbol{k}$ on the sublattice index $l = (1, 2, \ldots, n)$, and the Bloch Hamiltonian $\mathcal{H}(\boldsymbol{k})$ is the $2n \times 2n$ Hermitian matrix. If the energy bands $\pm E_m(\boldsymbol{k})$ obtained by diagonalizing $\mathcal{H}(\boldsymbol{k})$ are symmetric about the central zero-energy level, there should exist a chiral operator Γ that satisfies $\Gamma \mathcal{H}(\boldsymbol{k}) \Gamma^{\dagger} = -\mathcal{H}(\boldsymbol{k})$. In the basis that makes Γ diagonal, the operators are represented as

$$\Gamma = \begin{pmatrix} I & 0 \\ 0 & -I \end{pmatrix}, \quad \mathcal{H}(\boldsymbol{k}) = \begin{pmatrix} 0 & D(\boldsymbol{k}) \\ D^{\dagger}(\boldsymbol{k}) & 0 \end{pmatrix}, \quad (1)$$

where $D(\boldsymbol{k})$ is the $n_1 \times n_2$ matrix in general, and there are at least $|n_1 - n_2|$ zero modes, while for our Hamiltonian, $n_1 = n_2 = n$. The eigenvectors of Γ with eigenvalues ± 1 take the form $(\boldsymbol{\alpha}_m(\boldsymbol{k}), \boldsymbol{0})^T$ and $(\boldsymbol{0}, \boldsymbol{\beta}_m(\boldsymbol{k}))^T$. Since they satisfy $D(\boldsymbol{k}) \boldsymbol{\beta}_m(\boldsymbol{k}) = E_m(\boldsymbol{k}) \boldsymbol{\alpha}_m(\boldsymbol{k})$ and $D^{\dagger}(\boldsymbol{k}) \boldsymbol{\alpha}_m(\boldsymbol{k}) = E_m(\boldsymbol{k}) \boldsymbol{\beta}_m(\boldsymbol{k})$, the energy eigenstates of $\mathcal{H}(\boldsymbol{k})$ for $\pm E_m(\boldsymbol{k})$ are their bonding or antibonding states given as

$$|\psi_{\pm m}(\boldsymbol{k})\rangle \propto \begin{pmatrix} \boldsymbol{\alpha}_m(\boldsymbol{k}) \\ \boldsymbol{0} \end{pmatrix} \pm \begin{pmatrix} \boldsymbol{0} \\ \boldsymbol{\beta}_m(\boldsymbol{k}) \end{pmatrix}, \quad (2)$$

where Γ interchanges them. The reason why we find a CS in the bipartite and BdG systems is that due to the equivalence of two sublattices or the superconducting pairs, the Bloch basis is trivially classified into two equivalent bipartite groups. In our system, the CS is invisible since the nonbipartite lattice
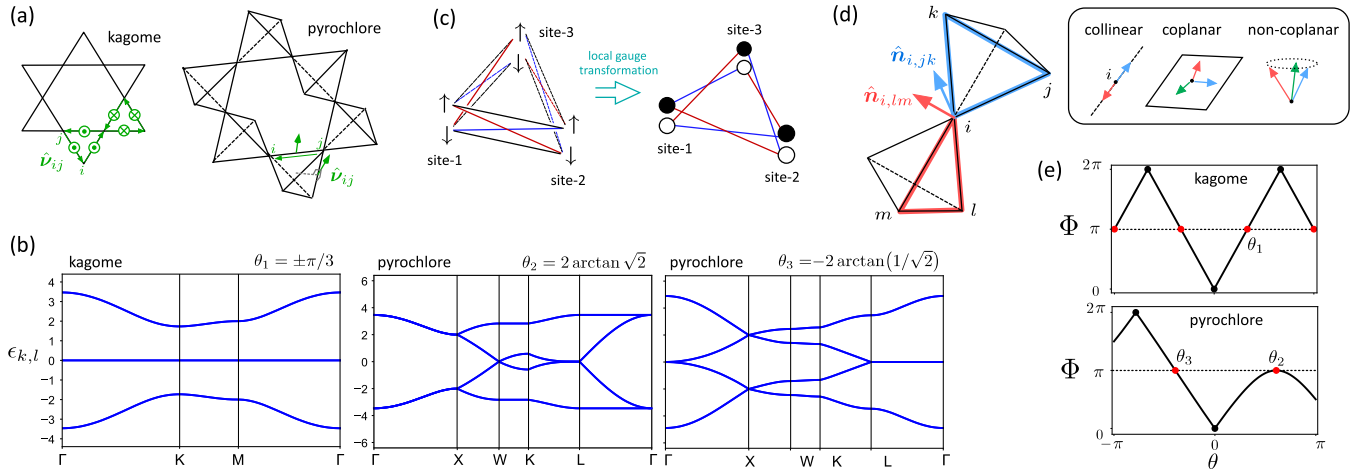
FIG. 1. (a) Kagome and pyrochlore lattices. The rotation axis $\hat{\boldsymbol{v}}_{ij}$ of the SU(2) gauge field is perpendicular to the bond and to the perpendicular bisector that crosses the center of the triangle/hexagon for the kagome/pyrochlore, and its direction depends on the order $j \to i$. (b) Chiral symmetric band structures are shown at $\theta = \theta_1 = \pm \pi/3$ and $\pm \pi$ for the kagome lattice and $\theta_2 = 2 \arctan \sqrt{2}$, $\theta_3 = -2 \arctan(1/\sqrt{2})$ for the pyrochlore lattice, where $\lambda/t_0 = \tan(\theta/2)$. (c) Schematic illustration of the original representation [Eq. (3)] with up/down spins and the transformed one with white/black circles. The latter has a bipartite-hopping structure on a triangle. (d) The Wilson loop operator rotates the spins when hopping around the $C_{i,jk}$ loop by Φ about the $\hat{\boldsymbol{n}}_{i,jk}$ axis. (e) Φ for the kagome and pyrochlore lattices. At the CS points, $\theta_1, \theta_2, \theta_3$, we find $\Phi = \pi$.

and the SOC mixes the up- and down-spin electrons between neighboring sites in a nontrivial manner where even a spin is no longer a good quantum number. We finally find that the local gauge transformation can untangle such a complexity and gives a proper basis set that is divided into bipartite groups.

SOC Hamiltonian on a nonbipartite lattice. We consider a tight-binding Hamiltonian defined on the kagome and pyrochlore lattices given as

$$\mathcal{H} = -t \sum_{\langle i,j \rangle} \boldsymbol{c}_i^\dagger U_{ij} \boldsymbol{c}_j + \text{H.c.}, \qquad (3)$$

where $\boldsymbol{c}_i = (c_{i\uparrow}, c_{i\downarrow})^{\text{T}}$ is the annihilation operator of an electron at site i, and the summation is taken over the neighboring pairs of sites $\langle i, j \rangle$. $\boldsymbol{\sigma} = (\sigma_x, \sigma_y, \sigma_z)$ are Pauli matrices and the hopping amplitude is set to unity, $t = 1$. When the electron hops from site j to the nearby site i, its spin rotates by angle θ about the $\hat{\boldsymbol{v}}_{ij}$ axis, which is expressed by the SU(2) gauge field $U_{ij} = \exp[-i\frac{\theta}{2}\hat{\boldsymbol{v}}_{ij} \cdot \boldsymbol{\sigma}]$, where $\hat{\boldsymbol{v}}_{ji} = -\hat{\boldsymbol{v}}_{ij}$ and $U_{ji} = U_{ij}^\dagger$. The unit vector $\hat{\boldsymbol{v}}_{ij}$ is determined by the lattice symmetry, and points to the direction perpendicular to the plane for the kagome lattice [28], while points in different directions perpendicular to the bond i-j for the pyrochlore lattice [29] [see Fig. 1(a) and Supplemental Sec. I [30]]. Our lattice has an inversion symmetry, but our theory is applied to cases of broken inversion symmetry. The origin of the SU(2) gauge field is the SOC [31–34]; In $4d$ and $5d$ electron systems, the interplay of strong *atomic* SOC and the crystal field enforces the reconstruction of energy levels on each site, and often the Kramers doublets labeled by the spin index σ form valence bands [35–38]. The d^5 pyrochlore oxides such as $A_2\text{Ir}_2\text{O}_7$ [39–42] and $\text{Lu}_2\text{Rh}_2\text{O}_7$ [43] have such doublets. In addition, $A_2\text{Os}_2\text{O}_7$ [44,45] and CsW_2O_6 [46] of different valences but in a trigonal crystal field belong to this category [37,47]. Since the spin momentum σ is a combination of orbital angular mo-

mentum and electron-spin momentum, the electrons can hop between orbitals having different spins as $i\lambda c_{i\alpha}^\dagger (\hat{\boldsymbol{v}}_{ij} \cdot \boldsymbol{\sigma})_{\alpha\beta} c_{j\beta}$. By combining this term with the ordinary hopping term $-t_0 c_{i\alpha}^\dagger c_{j\alpha}$, the form Eq. (3) is obtained as $t = \sqrt{t_0^2 + \lambda^2}$ and $\theta = 2 \arctan(\lambda/t_0)$. In Supplemental Sec. II [30], we derive θ microscopically using realistic values of the material data of $\text{Cd}_2\text{Os}_2\text{O}_7$, CsW_2O_6, and $\text{Pr}_2\text{Ir}_2\text{O}_7$ and find that they can afford CS.

SOC-induced chiral symmetry. As shown in Fig. 1(b), the energy band structures $\epsilon_{k,l}$ of Eq. (3) have CS at $\theta_1 = \pm \pi/3$, $\pm \pi$ for the kagome lattice and $\theta_2 = 2 \arctan \sqrt{2}$, $\theta_3 = -2 \arctan(1/\sqrt{2})$ for the pyrochlore lattice. To understand its origin, we need to find the form of two groups of basis sets that give ± 1 eigenvalues of Γ [see Eq. (1)]. Such a basis set is invisible since our lattices consist of triangles and in Eq. (3) the up- and down-spin electrons mix via U_{ij}. We set our goal to transform this basis set as in Fig. 1(c) to those having a bipartite hopping shown in the white and black circles; the white electron on site 1 hops to site 2 and to site 3 by successively changing its color between white and black, and comes back to site 1 as black. Going around the triangle twice, the initial configuration is recovered. We obtain this picture in the end by using the Wilson loop operator and constructing a chiral operator.

Gauge invariants. We now define a parameter that detects the CS. To do so, we need to characterize the nature of the SU(2) gauge. However, the values of θ and $\hat{\boldsymbol{v}}_{ij}$ in U_{ij} change if we apply a typical local gauge transformation $\boldsymbol{c}_i \to V_i \boldsymbol{c}_i$, where V_i denotes the SU(2) rotation of the quantized axis at site i. This change is only a matter of representation of the Hamiltonian and the band structure remains unchanged, i.e., gauge invariant. The parameter detecting the CS should have a one-to-one correspondence with the band structure and should be gauge invariant. The trace of the Wilson loop operator is known to be gauge invariant. The operator is constructed by

the path-ordered product of the SU(2) gauge field along the closed loop [27,28,34] $C_{i,jk} : i \rightarrow j \rightarrow k \rightarrow i$ [see Fig. 1(d)] as

$$P(C_{i,jk}) = U_{ik}U_{kj}U_{ji} = \exp\left[-i\frac{\Phi}{2}\hat{\boldsymbol{n}}_{i,jk} \cdot \boldsymbol{\sigma}\right], \qquad (4)$$

where Φ and $\hat{\boldsymbol{n}}_{i,jk}$ are the rotation angle and rotation axis, respectively, when the electron circles along the loop $C_{i,jk}$. Figure 1(e) shows Φ, which is gauge invariant, as a function of θ for the two lattices. By comparing it with the band structures, we find that the CS is characterized by $\Phi = \pi$. For the kagome lattice, Φ and band structures are the same between $\pm\theta$, but not for the pyrochlore lattice. This is because $\hat{\boldsymbol{v}}_{ij}$ is common to all bonds for the former and not for the latter, and accordingly, the U_{ij}'s of different bonds are commutative/noncommutative for the former/latter, which we denote the Abelian/non-Abelian case. We comment that these two should be rigorously distinguished as such that there exists a gauge that makes the SU(2) gauge fields commutative in the Abelian case and there is no such gauge in the non-Abelian case. If the definition of non-Abelian depends on the choice of gauge [48], it does not give a particular difference from the Abelian case about the gauge-invariant band structures or topological properties (see Supplemental Sec. III [30]). When $\Phi = 2\pi$, the flat band is formed by the SOC in both lattices [47]. Such a Wilson loop can be defined for different lengths as far as it consists of an odd number of bonds.

For the non-Abelian case, there should be another gauge-invariant quantity that distinguishes the positive and negative θ, which is the scalar product $\hat{\boldsymbol{n}}_{i,jk} \cdot \hat{\boldsymbol{n}}_{i,lm}$ around site i defined for different loops $C_{i,jk}$ and $C_{i,lm}$. Although $\hat{\boldsymbol{n}}_{i,jk}$ is not gauge invariant, their relative angle is invariant [see Fig. 1(d) and the proof in Supplemental Sec. III A [30]] [27]. Using this fact, we can classify the states into four cases, which we call trivial, collinear, coplanar, and noncoplanar cases. For the trivial case, $\Phi = 0, 2\pi$, the axis $\hat{\boldsymbol{n}}_{i,jk}$ is not defined since $P(C_{i,jk}) \propto I$. For $\Phi \neq 0, 2\pi$, if all $\hat{\boldsymbol{n}}_{i,jk}$ with different jk's for the same i are parallel we call it collinear, or if they are in the same plane we call it coplanar, and otherwise, it is noncoplanar [see the inset of Fig. 1(d)]. When the system is Abelian, it corresponds to either a collinear or trivial case. The non-Abelian case can be examined by comparing the two CS in Fig. 1(b): θ_2 is collinear and θ_3 is coplanar.

Chiral operator. The general form of the local gauge transformation is $V_j = \exp[-i\frac{\varphi_j}{2}\hat{\boldsymbol{m}}_j \cdot \boldsymbol{\sigma}]$, which rotates the spin quantization axis at site j by an angle φ_j about the axis $\hat{\boldsymbol{m}}_j$. If one could find the particular form of V_j that fulfills

$$V_i U_{ij} V_j^\dagger = -U_{ij}, \qquad (5)$$

one can construct a chiral operator satisfying $\Gamma^2 = +I$ as

$$\Gamma = i \oplus_{j=1}^n V_j, \qquad (6)$$

for which we immediately find $\Gamma\mathcal{H}(\boldsymbol{k})\Gamma^\dagger = -\mathcal{H}(\boldsymbol{k})$. To find such V_j we remind that the Wilson loop operator in Eq. (4) is obtained by the product of three U_{ij}'s. Accordingly, the chiral operation that changes the sign of U_{ij}'s will change the sign of $P(C_{i,jk})$. Since $\Phi = \pi$ at the CS point, the sign change is attained by the conversion of the axis via Eq. (5) as $\hat{\boldsymbol{n}}_{i,jk} \rightarrow -\hat{\boldsymbol{n}}_{i,jk}$. Namely, we need to set $\varphi_i = \pi$ and $\hat{\boldsymbol{m}}_i \perp \hat{\boldsymbol{n}}_{i,jk}$
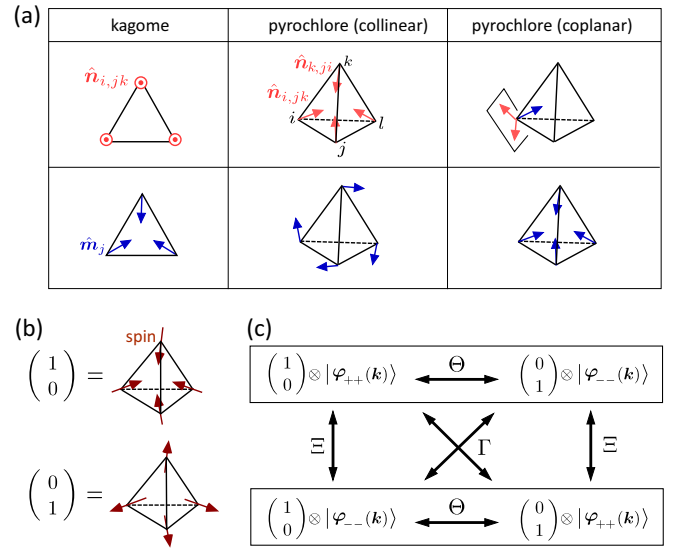

FIG. 2. (a) Vectors $\hat{\boldsymbol{n}}_{i,jk}$ and $\hat{\boldsymbol{m}}_j$ on the kagome and pyrochlore lattices with CS. Three or four sets of $\hat{\boldsymbol{m}}_j$ are not independent, but they can be rotated simultaneously in a plane perpendicular to $\hat{\boldsymbol{n}}_{i,jk}$ (kagome, pyrochlore collinear) or made upside down (pyrochlore coplanar). (b) All-in and all-out spin configurations forming a chiral pair, corresponding to the white and black circled basis in Fig. 1(c). (c) Relationships of four different energy eigenstates of the pyrochlore bands (collinear-type CS) that interchange by the TRS, PHS, and CS operations.

for all different $C_{i,jk}$'s around site i. It follows that $\hat{\boldsymbol{m}}_i$ can be defined when and only when $\hat{\boldsymbol{n}}_{i,jk}$'s on site i are either collinear or coplanar. Note that $\hat{\boldsymbol{m}}_j$ of different sites j are not independent and determined sequentially to satisfy $U_{ij} \rightarrow -U_{ij}$ (see Supplemental Sec. III B [30]). To summarize, the chiral operator Γ that satisfies Eq. (1) can be constructed when the Wilson loop operators satisfy (i) $\Phi = \pi$, and (ii) $\hat{\boldsymbol{n}}_{i,jk}$ is collinear or coplanar, where we can write down the explicit form as $iV_j = i \exp[-i\frac{\pi}{2}\hat{\boldsymbol{m}}_j \cdot \boldsymbol{\sigma}] = \hat{\boldsymbol{m}}_j \cdot \boldsymbol{\sigma}$.

Figure 2(a) shows an example of $\hat{\boldsymbol{m}}_j$ for three different CSs. Then, Eq. (6) indicates that in the basis that diagonalizes Γ, the up/down spin under the local quantization axis is parallel/antiparallel to $\hat{\boldsymbol{m}}_j$. Because of the block off-diagonal form of the Hamiltonian in Eq. (1), the electrons always turn over their spins when hopping. Namely, the up/down-spin basis forms a fictitious bipartite connection which we discussed in Fig. 1(c).

Emergent sublattice pseudospins. In the CS Hamiltonian Eq. (1), we find $D^\dagger(\boldsymbol{k}) \neq D(\boldsymbol{k})$ in general, but our collinear case shows $D^\dagger(\boldsymbol{k}) = D(\boldsymbol{k})$ (Supplemental Sec. IV [30]). Then, for $\boldsymbol{\varphi}_m(\boldsymbol{k})$ that satisfies $D(\boldsymbol{k})\boldsymbol{\varphi}_m(\boldsymbol{k}) = E_m\boldsymbol{\varphi}_m(\boldsymbol{k})$, we find $\mathcal{H}(\boldsymbol{k})|\psi_{\pm m}(\boldsymbol{k})\rangle = \pm E_m|\psi_{\pm m}(\boldsymbol{k})\rangle$, with $|\psi_{\pm m}(\boldsymbol{k})\rangle$ in Eq. (2) having $\boldsymbol{\alpha}_m(\boldsymbol{k}) = \boldsymbol{\beta}_m(\boldsymbol{k}) = \boldsymbol{\varphi}_m(\boldsymbol{k})$.

Here, $\hat{\boldsymbol{m}}_j$ gives the quantization axis whose up/down represents the black/white circles of Fig. 1(c). In this construction, the eigenstates of the Hamiltonian is the product of spin and sublattice parts given as $(1, \pm 1) \otimes \boldsymbol{\varphi}_m(\boldsymbol{k})$, and the spin part corresponds to the all-in and all-out spin configurations shown in Fig. 2(b). The sublattice (orbital) degrees of freedom in $D(\boldsymbol{k})$ show some hidden symmetries; for the kagome lattice,

TABLE I. The effect of perturbations on TRS, PHS, and CS. The absence of symmetry is denoted as 0, and the presence of TRS or PHS is denoted as ± 1 according to Θ^2, $\Xi^2 = \pm I$, and that of CS as 1. The last column shows the symmetry class the Hamiltonian belongs to [3].

Perturbation	TRS	PHS	CS	AZ class
Magnetic field	0	0	0/1	A/AIII
On-site potential	-1	0	0	AII
Bond modulation	-1	$+1$	1	DIII

$D(\boldsymbol{k}) = \boldsymbol{R}(\boldsymbol{k}) \cdot \boldsymbol{S}$, where $\boldsymbol{S}$ is the spin-1 operator in the 3×3 matrix representation (see Supplemental Sec. IV [30]). The eigenstate $\boldsymbol{\varphi}_m(\boldsymbol{k})$ of the sublattice degrees of freedom has three states with $S = 1, 0, -1$. The energy bands carry the sublattice pseudospins that point parallel/antiparallel to the SO(3) vector $\boldsymbol{R}(\boldsymbol{k})$ whose direction varies with $\boldsymbol{k}$, which reminds us of a Rashba-Dresselhaus Hamiltonian [49,50]. Similar sublattice pseudospins consisting of two spin-1/2's are obtained for the pyrochlore case [51].

We briefly comment on the chiral zero modes. The doubly degenerate flat band [Fig. 1(b)] in our kagome lattice appears trivially since n is odd and CS is present. In the well-known case on a Lieb lattce [52] they appear since $n_1 \neq n_2$ in Eq. (1). For the pyrochlore lattice, the W and L point contacts for θ_2 and the Γ-L nodal line for θ_3 are the essential degeneracies [53] protected by the CS and lattice symmetry (see Supplemental Sec. IV [30]).

Symmetries and perturbations. We see how TRS (time-reversal operator Θ), PHS (charge conjugation operator Ξ), and CS (Γ) in our system act together as $\Xi = \Gamma\Theta$. At the chiral symmetric points, $\Theta^{-1}\Gamma\Theta = -\Gamma$, which indicates $\Xi^2 = +I$, and by combining it with $\Theta^2 = -I$, our system is found to belong to class DIII. In the collinear case, these operators clarify the existence of the particle-hole pair [see Fig. 2(c) for the pyrochlore lattice at $\theta = \theta_2$]; Γ/Ξ flips only the true spin (on a local quantization axis)/the sublattice pseudospin and interchanges the energy level $\pm E_m$ [54].

Another interest is how robust our CS is against the perturbations. Using the Wilson loop operator, we examine three types of perturbations in Table I (see Supplemental Sec. V [30]). Remarkably, the magnetic field (Zeeman terms) breaks both TRS and PHS, but does not necessarily break the CS, i.e., although CS is knit to spins it does not require spin-conversion symmetry. This differs from graphene, where the field generally preserves the CS [55,56]. The on-site potential keeps the TRS but breaks PHS, and CS is always broken. The bond modulation breaks the spatial inversion symmetry and the band degeneracy is lifted, but since it breaks neither TRS nor PHS, the CS is preserved. Several examples of band structures under these perturbations are shown in Fig. 3(a).

We show in Fig. 3(b) the bands with on-site potentials and the bond modulation obtained by taking the interkagome plane direction as an open boundary. The CS state belonged to class DIII transforms into class AII, where a strong TI is expected [57]. Indeed, we see a clear indication of the edge modes.
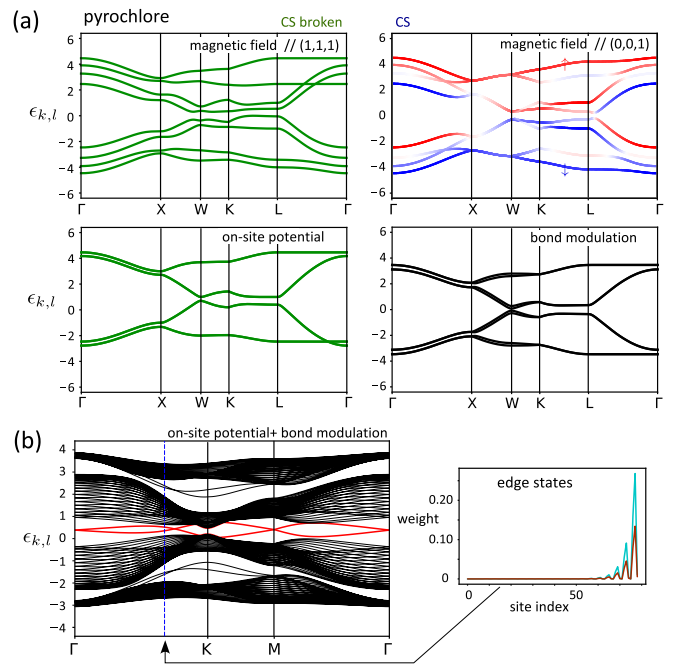

FIG. 3. (a) Band structures of the pyrochlore lattices when we add to Eq. (3) the perturbations shown in Table I: magnetic field $h = 1$ in two different directions, on-site potentials with $(w_1, w_2, w_3, w_4) = (1, 1, 1, 0.4)$, bond modulations. Left/right bands have non-CS/CS. In the upper-right CS band we show the density plot of the magnetic moment showing clear spin splitting (red/blue are the up/down-spin moments). (b) Recalculated bands with on-site potentials and bond modulation, taking the inter-kagome-plane direction as an open boundary, where we find an edge state, indicated in red lines since this case corresponds to the strong TI in class AII. Distributions of edge modes in the open directions. Up/down spins shown in cyan/brown belong to one mode. For the other mode, the distribution of each spin is opposite.

In conclusion, we found a framework for generalizing chiral symmetry; it can be straightforwardly extended to systems of multiplet-based models and simulations [58]. The local gauge transformation to a properly chosen site-dependent "quantization axis" can untangle the complexity of the original Hamiltonian, and the resultant basis sets can be divided into subgroups that form a bipartite hopping structure. The Wilson loop operator is useful to search for such a transformation.

The consequences of the CS in a SOC system can be rich. For example in Fig. 3(a), the CS bands in a magnetic field carry true magnetic moments that change their direction with $\boldsymbol{k}$. Unlike Rashba systems [49,50], these bands have particle-hole symmetry that may yield unexpected transport properties, similarly to the Mott-to-anomalous Hall phase that makes use of the band inversion [59]. A more exotic platform is the zero-energy flat bands in the kagome lattice [Fig. 1(b)]. Similarly to twisted bilayer graphene [16–19], they are protected by the underlying CS, but on top of that, the electrons on our flat bands carry spatially varying polarized moments. The CS-protected flat bands can further be engineered by introducing site vacancies as another parameter [20]. Importantly, such electrons in the "strong correlation limit" are

considered as the source of unconventional superconductivity [21,22], and this feature sustains even when the material parameters slightly break the CS. In particle physics, one can consider an analog of our SU(2) model and its consequences in the lattice gauge theories to understand the gravitational spin connection in curved space-time, where the SU(2) gauge emerges by a local Lorentz transformation.

[1] J. C. Slater, *Symmetry and Energy Bands in Crystals* (Dover, New York, 1972).

[2] L. Landau, E. Lifshitz, and M. Pitaevskii, *Statistical Physics* (Butterworth-Heinemann, New York, 1999).

[3] A. P. Schnyder, S. Ryu, A. Furusaki, and A. W. W. Ludwig, Classification of topological insulators and superconductors in three spatial dimensions, Phys. Rev. B **78**, 195125 (2008).

[4] A. Kitaev, Periodic table for topological insulators and superconductors, AIP Conf. Proc. **1134**, 22 (2009).

[5] J. Kruthoff, J. de Boer, J. van Wezel, C. L. Kane, and R.-J. Slager, Topological Classification of Crystalline Insulators through Band Structure Combinatorics, Phys. Rev. X **7**, 041069 (2017).

[6] X. Wen and A. Zee, Winding number, family index theorem, and electron hopping in a magnetic field, Nucl. Phys. B **316**, 641 (1989).

[7] W. P. Su, J. R. Schrieffer, and A. J. Heeger, Solitons in Polyacetylene, Phys. Rev. Lett. **42**, 1698 (1979).

[8] W. P. Su, J. R. Schrieffer, and A. J. Heeger, Soliton excitations in polyacetylene, Phys. Rev. B **22**, 2099 (1980).

[9] S. Ryu and Y. Hatsugai, Topological Origin of Zero-Energy Edge States in Particle-Hole Symmetric Systems, Phys. Rev. Lett. **89**, 077002 (2002).

[10] Y. Hatsugai, T. Fukui, and H. Aoki, Topological aspects of graphene, Eur. Phys. J. Spec. Top. **148**, 133 (2007).

[11] Y. Hatsugai, Bulk-edge correspondence in graphene with/ without magnetic field: Chiral symmetry, Dirac fermions and edge states, Solid State Commun. **149**, 1061 (2009).

[12] H. Aoki and M. S. Dresselhaus, *Physics of Graphene* (Springer, Berlin, 2013).

[13] E. McCann and V. I. Fal'ko, Landau-Level Degeneracy and Quantum Hall Effect in a Graphite Bilayer, Phys. Rev. Lett. **96**, 086805 (2006).

[14] M. I. Katsnelson and M. F. Prokhorova, Zero-energy states in corrugated bilayer graphene, Phys. Rev. B **77**, 205424 (2008).

[15] M. Koshino, T. Morimoto, and M. Sato, Topological zero modes and Dirac points protected by spatial symmetry and chiral symmetry, Phys. Rev. B **90**, 115207 (2014).

[16] E. Suárez Morell, J. D. Correa, P. Vargas, M. Pacheco, and Z. Barticevic, Flat bands in slightly twisted bilayer graphene: Tight-binding calculations, Phys. Rev. B **82**, 121407(R) (2010).

[17] R. Bistritzer and A. H. MacDonald, Moire bands in twisted double-layer graphene, Proc. Natl. Acad. Sci. USA **108**, 12233 (2011).

[18] G. Trambly de Laissardière, D. Mayou, and L. Magaud, Numerical studies of confined states in rotated bilayers of graphene, Phys. Rev. B **86**, 125413 (2012).

[19] G. Li, A. Luican, J. M. B. L. dos Santos, A. H. C. Neto, A. Reina, J. Kong, and E. Y. Andrei, Observation of Van Hove singularities in twisted graphene layers, Nat. Phys. **6**, 109 (2010).

[20] M. S. M. de Sousa, F. Liu, F. Qu, and W. Chen, Vacancy-engineered flat-band superconductivity in holey graphene, Phys. Rev. B **105**, 014511 (2022).

[21] Y. Cao, V. Fatemi, A. Demir, S. Fang, S. L. Tomarken, J. Y. Luo, J. D. Sanchez-Yamagishi, K. Watanabe, T. Taniguchi, E. Kaxiras, R. C. Ashoori, and P. Jarillo-Herrero, Correlated insulator behaviour at half-filling in magic-angle graphene superlattices, Nature (London) **556**, 80 (2018).

[22] Y. Cao, V. Fatemi, S. Fang, K. Watanabe, T. Taniguchi, E. Kaxiras, and P. Jarillo-Herrero, Unconventional superconductivity in magic-angle graphene superlattices, Nature (London) **556**, 43 (2018).

[23] R. Gade, Anderson localization for sublattice models, Nucl. Phys. B **398**, 499 (1993).

[24] T. Kawarabayashi, Y. Hatsugai, T. Morimoto, and H. Aoki, Generalized chiral symmetry and stability of zero modes for tilted Dirac cones, Phys. Rev. B **83**, 153414 (2011).

[25] B. Li and A. A. Kovalev, Chiral topological insulator of magnons, Phys. Rev. B **97**, 174413 (2018).

[26] J. Verbaarschot, Spectrum of the QCD Dirac Operator and Chiral Random Matrix Theory, Phys. Rev. Lett. **72**, 2531 (1994).

[27] X.-G. Wen, *Quantum Field Theory of Many-Body Systems: From the Origin of Sound to an Origin of Light and Electrons* (Oxford University Press, Oxford, UK, 2004).

[28] S. K. Kim and J. Zang, U(1) symmetry of the spin-orbit coupled Hubbard model on the kagome lattice, Phys. Rev. B **92**, 205106 (2015).

[29] M. Kurita, Y. Yamaji, and M. Imada, Topological insulators from spontaneous symmetry breaking induced by electron correlation on pyrochlore lattices, J. Phys. Soc. Jpn. **80**, 044708 (2011).

[30] See Supplemental Material at http://link.aps.org/supplemental/10.1103/PhysRevB.108.L081106 for the details of the SOC Hamiltonian, evaluation of model parameters in materials, Wilson loop operator, symmetry analysis, and perturbation Hamiltonian, which includes Refs. [60,61].

[31] L. Shekhtman, O. Entin-Wohlman, and A. Aharony, Moriya's Anisotropic Superexchange Interaction, Frustration, and Dzyaloshinsky's Weak Ferromagnetism, Phys. Rev. Lett. **69**, 836 (1992).

[32] G. Guarnaccia and C. Noce, Hubbard model with spin-orbit coupling: Lattice gauge theory approach, Phys. Rev. B **86**, 064409 (2012).

[33] S. Zhu, Y.-Q. Li, and C. D. Batista, Spin-orbit coupling and electronic charge effects in Mott insulators, Phys. Rev. B **90**, 195107 (2014).

[34] S.-S. Zhang, H. Ishizuka, H. Zhang, G. B. Halász, and C. D. Batista, Real-space Berry curvature of itinerant electron systems with spin-orbit interaction, Phys. Rev. B **101**, 024420 (2020).

[35] B. J. Kim, H. Jin, S. J. Moon, J.-Y. Kim, B.-G. Park, C. S. Leem, J. Yu, T. W. Noh, C. Kim, S.-J. Oh, J.-H. Park, V. Durairaj, G. Cao, and E. Rotenberg, Novel $J_{eff} = 1/2$ Mott State Induced by Relativistic Spin-Orbit Coupling in Sr_2IrO_4, Phys. Rev. Lett. **101**, 076402 (2008).

[36] D. Uematsu, H. Sagayama, T.-H. Arima, J. J. Ishikawa, S. Nakatsuji, H. Takagi, M. Yoshida, J. Mizuki, and K. Ishii, Large trigonal-field effect on spin-orbit coupled states in a pyrochlore iridate, Phys. Rev. B **92**, 094405 (2015).

[37] D. I. Khomskii, K. I. Kugel, A. O. Sboychakov, and S. V. Streltsov, Role of local geometry in the spin and orbital structure of transition metal compounds, J. Exp. Theor. Phys. **122**, 484 (2016).

[38] T. Takayama, J. Chaloupka, A. Smerald, G. Khaliullin, and H. Takagi, Spin–orbit-entangled electronic phases in 4d and 5d transition-metal compounds, J. Phys. Soc. Jpn. **90**, 062001 (2021).

[39] D. Yanagishima and Y. Maeno, Metal-nonmetal changeover in pyrochlore iridates, J. Phys. Soc. Jpn. **70**, 2880 (2001).

[40] K. Matsuhira, M. Wakeshima, R. Nakanishi, T. Yamada, A. Nakamura, W. Kawano, S. Takagi, and Y. Hinatsu, Metal-insulator transition in pyrochlore iridates $Ln_2Ir_2O_7$ (Ln = Nd, Sm, and Eu), J. Phys. Soc. Jpn. **76**, 043706 (2007).

[41] T. F. Qi, O. B. Korneta, X. Wan, L. E. DeLong, P. Schlottmann, and G. Cao, Strong magnetic instability in correlated metallic $Bi_2Ir_2O_7$, J. Phys.: Condens. Matter **24**, 345601 (2012).

[42] T. Kondo, M. Nakayama, R. Chen, J. J. Ishikawa, E.-G. Moon, T. Yamamoto, Y. Ota, W. Malaeb, H. Kanai, Y. Nakashima, Y. Ishida, R. Yoshida, H. Yamamoto, M. Matsunami, S. Kimura, N. Inami, K. Ono, H. Kumigashira, S. Nakatsuji, L. Balents *et al.*, Quadratic Fermi node in a 3D strongly correlated semimetal, Nat. Commun. **6**, 10042 (2015).

[43] A. M. Hallas, A. Z. Sharma, C. Mauws, Q. Chen, H. D. Zhou, C. Ding, Z. Gong, M. Tachibana, P. M. Sarte, J. P. Attfield, G. M. Luke, and C. R. Wiebe, Coexistence of metallic and nonmetallic properties in the pyrochlore $Lu_2Rh_2O_7$, npj Quantum Mater. **4**, 9 (2019).

[44] J. Yamaura, K. Ohgushi, H. Ohsumi, T. Hasegawa, I. Yamauchi, K. Sugimoto, S. Takeshita, A. Tokuda, M. Takata, M. Udagawa, M. Takigawa, H. Harima, T. Arima, and Z. Hiroi, Tetrahedral Magnetic Order and the Metal-Insulator Transition in the Pyrochlore Lattice of $Cd_2Os_2O_7$, Phys. Rev. Lett. **108**, 247205 (2012).

[45] K. Kataoka, D. Hirai, A. Koda, R. Kadono, T. Honda, and Z. Hiroi, Pyrochlore oxide $Hg_2Os_2O_7$ on verge of metal–insulator boundary, J. Phys.: Condens. Matter **34**, 135602 (2022).

[46] Y. Okamoto, H. Amano, N. Katayama, H. Sawa, K. Niki, R. Mitoka, H. Harima, T. Hasegawa, N. Ogita, Y. Tanaka, M. Takigawa, Y. Yokoyama, K. Takehana, Y. Imanaka, Y. Nakamura, H. Kishida, and K. Takenaka, Regular-triangle trimer and charge order preserving the Anderson condition in

the pyrochlore structure of CsW_2O_6, Nat. Commun. **11**, 3144 (2020).

[47] H. Nakai and C. Hotta, Perfect flat band with chirality and charge ordering out of strong spin-orbit interaction, Nat. Commun. **13**, 579 (2022).

[48] Z. Gao and Z. Lan, Flat bands and $\mathbb{Z}_2$ topological phases in a non-Abelian kagome lattice, Phys. Rev. B **102**, 245133 (2020).

[49] E. I. Rashba, Properties of semiconductors with an extremum loop. 1. Cyclotron and combinational resonance in a magnetic field perpendicular to the plane of the loop, Sov. Phys. Solid State **2**, 1109 (1960).

[50] G. Dresselhaus, Spin-orbit coupling effects in zinc blende structures, Phys. Rev. **100**, 580 (1955).

[51] For the pyrochlore, $D(\boldsymbol{k}) = \boldsymbol{R}_1(\boldsymbol{k}) \cdot \boldsymbol{S}_1 + \boldsymbol{R}_2(\boldsymbol{k}) \cdot \boldsymbol{S}_2$, where $\boldsymbol{R}_j(\boldsymbol{k})$ is the SO(3) vector. $\boldsymbol{S}_1$ and $\boldsymbol{S}_2$ are the pseudo-spin-1/2 operators, which commute in the 4×4 representation (Supplemental Sec. IV [30]). Four $\boldsymbol{\varphi}_m(\boldsymbol{k})$ are classified by $(\boldsymbol{S}_1, \boldsymbol{S}_2)$ being parallel or antiparallel to $[\boldsymbol{R}_1(\boldsymbol{k}), \boldsymbol{R}_2(\boldsymbol{k})]$, and its eigenvalue is $[\sigma_1 |\boldsymbol{R}_1(\boldsymbol{k})| + \sigma_2 |\boldsymbol{R}_2(\boldsymbol{k})|]/2$.

[52] A. Ramachandran, A. Andreanov, and S. Flach, Chiral flat bands: Existence, engineering, and stability, Phys. Rev. B **96**, 161104(R) (2017).

[53] K. Asano and C. Hotta, Designing Dirac points in two-dimensional lattices, Phys. Rev. B **83**, 245125 (2011).

[54] It follows that Θ flips both and exchanges the energetically degenerate pairs of states. Since Ξ takes the role of pseudo-TRS for sublattice pseudospins, $\Xi^2 = +I$ prohibits the odd-numbered half-integer sublattice pseudospins. This explains why the pyrochlore lattice sublattice degrees of freedom explained in Ref. [51] are not described by a single pseudospin-3/2 but by the two pseudospin-1/2.

[55] A. J. M. Giesbers, U. Zeitler, M. I. Katsnelson, L. A. Ponomarenko, T. M. Mohiuddin, and J. C. Maan, Quantum-Hall Activation Gaps in Graphene, Phys. Rev. Lett. **99**, 206803 (2007).

[56] Y. Hatsugai, T. Kawarabayashi, and H. Aoki, Survival of sharp $n = 0$ Landau levels in massive tilted Dirac fermions: Role of the generalized chiral operator, Phys. Rev. B **91**, 085112 (2015).

[57] W. Witczak-Krempa, A. Go, and Y. B. Kim, Pyrochlore electrons under pressure, heat, and field: Shedding light on the iridates, Phys. Rev. B **87**, 155101 (2013).

[58] I. Bloch, J. Dalibard, and S. Nascimbène, Quantum simulations with ultracold quantum gases, Nat. Phys. **8**, 267 (2012).

[59] T. Devakul and L. Fu, Quantum Anomalous Hall Effect from Inverted Charge Transfer Gap, Phys. Rev. X **12**, 021031 (2022).

[60] K. I. Kugel, D. I. Khomskii, A. O. Sboychakov, and S. V. Streltsov, Spin-orbital interaction for face-sharing octahedra: Realization of a highly symmetric SU(4) model, Phys. Rev. B **91**, 155125 (2015).

[61] J. C. Slater and G. F. Koster, Simplified LCAO method for the periodic potential problem, Phys. Rev. **94**, 1498 (1954).